

Broadband Ground-Motion Simulation with Interfrequency Correlations

by Nan Wang,^{*} Rumi Takedatsu, Kim B. Olsen, and Steven M. Day

Abstract Ground-motion simulations can be viable alternatives to empirical relations for seismic hazard analysis when data are sparse. Interfrequency correlation is revealed in recorded seismic data, which has implications for seismic risk (Bayless and Abrahamson, 2018a). However, in many cases, simulated ground-motion time series, in particular those originating from stochastic methods, lack interfrequency correlation. Here, we develop a postprocessing method to rectify simulation techniques that otherwise produce synthetic time histories deficient in an interfrequency correlation structure. An empirical correlation matrix is used in our approach to generate correlated random variables that are multiplied in the frequency domain with the Fourier amplitudes of the synthetic ground-motion time series. The method is tested using the San Diego State University broadband ground-motion generation module, which is a broadband ground-motion generator that combines deterministic low-frequency and stochastic high-frequency signals, validated for the median of the spectral acceleration. Using our method, the results for seven western U.S. earthquakes with magnitude between 5.0 and 7.2 show that empirical interfrequency correlations are well simulated for a large number of realizations without biasing the fit of the median of the spectral accelerations to data. The best fit of the interfrequency correlation to data is obtained assuming that the horizontal components are correlated with a correlation coefficient of about 0.7.

Supplemental Material

Introduction

Numerical simulations can provide critical information for seismic hazard analysis at near-fault distances and for large-magnitude earthquakes where strong-motion records are sparse. Recent advances in simulation methods due to improved source characterization, accuracy of wave propagation methods, and available computational resources have increased potential benefits for seismic hazard assessment. Ground motions generated by many broadband simulation methods (e.g., Atkinson and Assatourians, 2015; Crempien and Archuleta, 2015; Graves and Pitarka, 2015; Olsen and Takedatsu, 2015) have been used as input for engineering applications. However, although these methods have been tuned to produce median spectral acceleration in good agreement with that from strong-motion data, less attention has been paid to their correlation behavior compared with empirical data (Bayless and Abrahamson, 2018a).

Seismic ground motions recorded from earthquakes reveal both interfrequency and spatial correlation. A number of studies have been done over the past decades for the

spatial correlation of response spectra (e.g., Wesson and Perkins, 2001; Boore *et al.*, 2003; Kawakami and Mogi, 2003; Wang and Takada, 2005; Goda and Hong, 2008; Jayaram and Baker, 2009; Esposito and Iervolino, 2011; Sokolov *et al.*, 2012; Loth and Baker, 2013; Sokolov and Wenzel, 2013; Markhvida *et al.*, 2018; Heresi and Miranda, 2019) and interfrequency correlations of response spectra (e.g., Baker and Cornell, 2006; Baker and Jayaram, 2008; Goda and Atkinson, 2009; Cimellaro, 2013; Abrahamson *et al.*, 2014; Akkar *et al.*, 2014; Azarbakht *et al.*, 2014; Baker and Bradley, 2017), as well as some recent studies for interfrequency correlations of Fourier spectra (e.g., Wharf, 2016; Stafford, 2017; Bayless and Abrahamson, 2019). In addition, many studies (e.g., Burks and Baker, 2014; Weatherill *et al.*, 2015; Stafford, 2017; Bayless and Abrahamson, 2018a) have demonstrated how seismic hazard assessment from simulations without such correlation can lead to underprediction of the seismic risk.

Stafford (2017) and Bayless and Abrahamson (2018a) both proposed techniques to incorporate interfrequency correlations into the Boore (2003) simulation method. The Boore (2003) method generates a windowed Gaussian noise, transformed into the frequency domain and shaped by the

^{*}Also at Institute of Geophysics and Planetary Physics, Scripps Institution of Oceanography, University of California San Diego, 9500 Gilman Drive, La Jolla, California 92093-0225 U.S.A.

deterministic Fourier amplitude spectrum (FAS) for a scenario. [Stafford \(2017\)](#) used a model that is developed using two as-recorded horizontal components of unsmoothed FAS. [Bayless and Abrahamson \(2018a\)](#) used an interfrequency model that is developed using a smoothed and orientation-independent FAS called effective amplitude spectrum (EAS, as described in the following sections). We choose to apply the model developed using the EAS, applied to each of the two horizontal components, because our simulations are performed separately for each component. In contrast to the two recent studies mentioned earlier, we optimize the results for the interfrequency correlation based on assumptions about the correlation of the two horizontal orthogonal components. Specifically, we find that incorporating two correlated FAS components can lead to a more accurate correlation structure in EAS, as described in the following sections.

The goal of this study is to develop a new approach for including interfrequency correlation in stochastic ground-motion simulations, and to demonstrate and validate the approach on an established and validated ground-motion simulation tool. We have selected the San Diego State University (SDSU) broadband ground-motion generation module ([Olsen and Takedatsu, 2015](#)) which is implemented on the Southern California Earthquake Center (SCEC) Broadband Platform (BBP) for this purpose. The SDSU BBP module participated in and passed the SCEC BBP validation exercise ([Dreger, et al., 2015](#); [Goulet et al., 2015](#)). The focus of this exercise was on validating simulated median pseudospectral accelerations (PSAs) for earthquakes in western and eastern United States and Japan, as well as Next Generation Attenuation ground-motion prediction equations (GMPEs). The stochastic component of the SDSU method has undergone extensive calibration with respect to PSA using GMPEs and strong-motion data, aiming at improving the prediction of ground motions. However, the SDSU module was designed to provide satisfactory fits to data for median ground motions only, lending itself as an appropriate testbed for incorporating interfrequency correlation.

PSA has traditionally been the preferred metric in earthquake engineering. However, PSA for a given response frequency depends (nonlinearly) on ground-motion amplitudes over a range of frequencies. On the other hand, the FAS is simply obtained by Fourier transform of the time series and can therefore be used more directly in ground-motion simulation of time histories. This extends to interfrequency correlations as well, as shown by [Bayless and Abrahamson \(2019\)](#) for ground motions from the Pacific Earthquake Engineering Research Center Next Generation Attenuation-West2 Project (NGA-West2) database.

This article starts by reviewing the intensity measure and the empirical covariance matrix for interfrequency correlations that we used. We then explain and verify our approach to compute the correlation, and demonstrate how the interfrequency correlation coefficients are applied to the SDSU module.

FAS and EAS

The FAS is the amplitude spectrum of the Fourier transform of the acceleration time series. The EAS defined by [Goulet et al. \(2018\)](#) as

$$\text{EAS}(f) = \sqrt{\frac{1}{2}[\text{FAS}_{\text{HC1}}^2(f) + \text{FAS}_{\text{HC2}}^2(f)]} \quad (1)$$

is used as the intensity measure in our study. In equation (1), FAS_{HC1} and FAS_{HC2} are the FAS of the two as-recorded horizontal components of a three-component acceleration time series, and f is the frequency in hertz. The EAS is independent of the recording instrument's orientation. The EAS is smoothed using the \log_{10} -scale [Konno and Ohmachi \(1998\)](#) smoothing window selected by [Kottke et al. \(2018\)](#)

$$W(f) = \left(\frac{\sin(b \log(f/f_c))}{b \log(f/f_c)} \right)^4, \quad (2)$$

in which W is the weight defined at frequency f for a window with center frequency f_c , and $b = \frac{2\pi}{b_w} = 60\pi$ in which b_w is the smoothing window bandwidth in \log_{10} units. For more details on the smoothing technique, the reader is referred to [Kottke et al. \(2018\)](#).

Interfrequency Correlations of Within-Event Residual

We follow the notation defined by [Al Atik et al. \(2010\)](#)

$$y_{es} = \mu_{es} + \delta B_e + \delta W_{es}, \quad (3)$$

in which y_{es} is the natural logarithm of the ground-motion intensity measure observed at station s during earthquake e , and μ_{es} is the mean prediction of the natural logarithm of the intensity measure. δB_e is the between-event residual (or interevent residual), representing the average shift of the observed ground motion for an individual earthquake e from the population mean prediction. δW_{es} is the within-event residual (or intraevent residual), depicting the misfit between an individual observation at station s from the earthquake-specific mean prediction. The source effect average (over all azimuths) is described by the between-event residual that reflects the influence of factors such as stress drop and variation of slip in time and space that cannot be captured by the inclusion of magnitude, faulting style, and source depth in the mean prediction. Azimuthal variations in source, path, and site effects are described by the within-event residual that reflects the influence of factors such as crustal heterogeneity, deeper geological structure, and near-surface layering that cannot be captured by a simple distance metric and a site-classification based on the average shear-wave velocity ([Al Atik et al., 2010](#)). These residuals are normally distributed with zero mean and are uncorrelated with each other.

In this study, we focus on within-event variability only. Although between-event variability conceptually can be treated in a similar fashion, it would require extensive changes

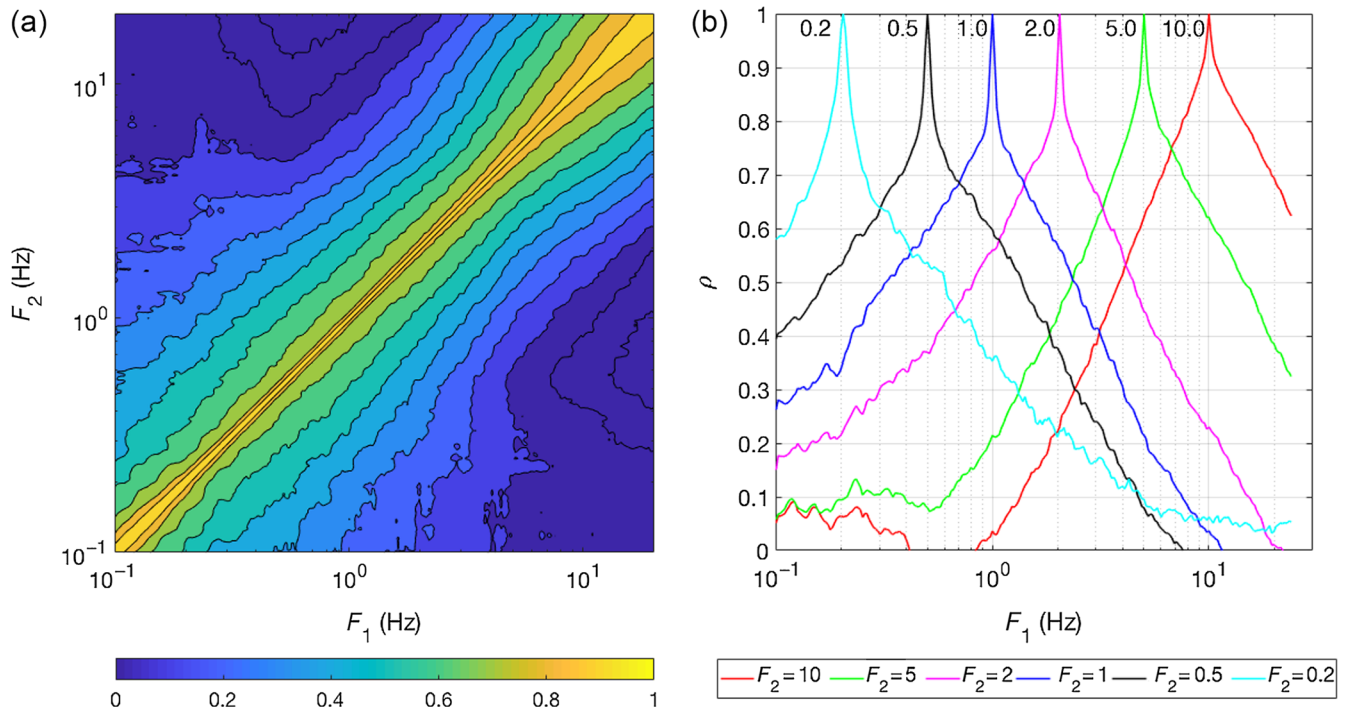


Figure 1. (a) Empirical within-event residual interfrequency correlation coefficients contour plot and (b) cross section versus frequency at conditioning frequencies 0.2, 0.5, 1, 2, 5, and 10 Hz. Modified from Bayless and Abrahamson (2019). The color version of this figure is available only in the electronic edition.

to the target code for our analysis (the SDSU broadband module) as well as current computational procedures on the SCEC BBP. For these reasons, we leave the between-event variability for future work.

We target the EAS within-event residual through epsilon (\$\epsilon\$),

$$\epsilon(f) = \frac{\delta W_{es}(f)}{\varphi(f)} = \frac{\ln \text{EAS}_{es}(f) - \mu_{\ln \text{EAS}_{es}}(f) - \delta B_e}{\varphi(f)}, \quad (4)$$

the within-event residual normalized by its standard deviation \$\varphi\$. The value of the within-event residual of EAS depends on frequency \$f\$. By the normalization, epsilon is standard normally distributed.

For a given set of observations, the values of \$\epsilon\$ at neighboring frequencies (\$f\$) are probabilistically correlated. If a ground-motion intensity measure is stronger than average at a certain frequency, it tends to also be stronger at nearby frequencies; however, the \$\epsilon\$ values are weakly correlated if the frequency pair are widely separated (Bayless and Abrahamson, 2018a). The correlation coefficient of \$\epsilon\$ at two frequencies \$f_1\$ and \$f_2\$ can be estimated by the maximum-likelihood estimator (Kutner et al., 2004) using the Pearson product-moment correlation coefficient (Fisher, 1958)

$$\rho_{\epsilon(f_1)\epsilon(f_2)} = \frac{\sum_{i=1}^n (\epsilon_i(f_1) - \overline{\epsilon(f_1)}) (\epsilon_i(f_2) - \overline{\epsilon(f_2)})}{\sqrt{\sum_{i=1}^n (\epsilon_i(f_1) - \overline{\epsilon(f_1)})^2} \sqrt{\sum_{i=1}^n (\epsilon_i(f_2) - \overline{\epsilon(f_2)})^2}}, \quad (5)$$

in which \$n\$ is the number of observations, \$\epsilon_i(f_1)\$ and \$\epsilon_i(f_2)\$ represent the \$i\$th observation of \$\epsilon\$ at frequencies \$f_1\$ and \$f_2\$, respectively, \$\overline{\epsilon(f_1)}\$ and \$\overline{\epsilon(f_2)}\$ are their sample means, and the expectations of \$\epsilon(f_1)\$ and \$\epsilon(f_2)\$ are both zero. This correlation is important when simulated time histories are used for seismic risk analysis because variability in the dynamic structural response will be underestimated if the interfrequency correlation in simulated ground motions is unrealistically low (Bayless and Abrahamson, 2018a).

Bayless and Abrahamson (2019) generated an empirical estimate of \$\rho\$ for the EAS within-event residual (with the within-event residual partitioned into site-to-site and within-site residuals) using the NGA-West2 database (regression from shallow crustal earthquakes, with \$M > 3\$) at frequencies from 0.1 to 24 Hz. The epsilon at each frequency, which was determined in the Bayless and Abrahamson (2018b) EAS model regression, was calculated from the individual EAS values and the earthquake-specific smoothed EAS median model for each recorded event at each station. Then, \$\rho_{\epsilon(f_1)\epsilon(f_2)}\$ was calculated for each pair of frequencies \$f_1\$ and \$f_2\$. Figure 1 shows the empirical correlation coefficients. This empirical estimation for the interfrequency correlation coefficients of the within-event residual is applied into the implementation method described in the following section.

The SDSU Broadband Ground-Motion Generation Module (SDSU Module)

The SDSU module is a hybrid method that merges deterministic low-frequency (LF) synthetics and high-frequency

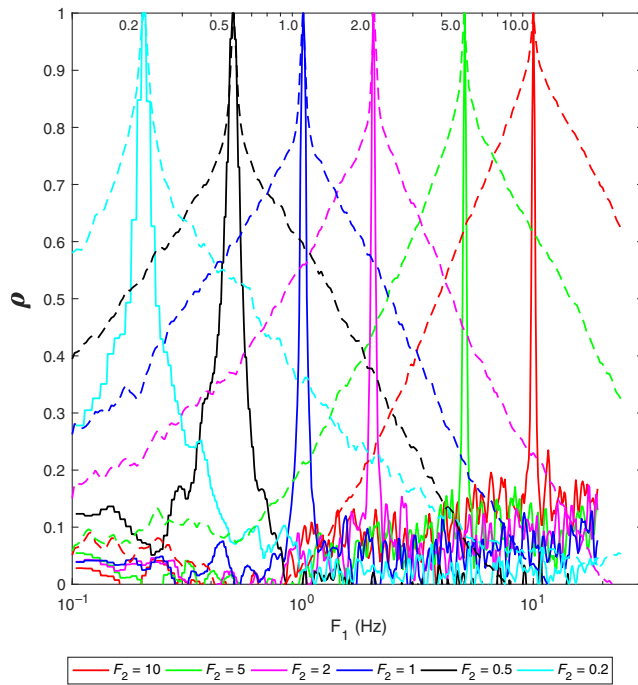


Figure 2. Interfrequency correlation coefficients of epsilon at reference frequencies 0.2, 0.5, 1, 2, 5, and 10 Hz from the current San Diego State University (SDSU) module using 50 source realizations of the Loma Prieta earthquake (solid lines), compared to the empirical correlation coefficients (Bayless and Abrahamson, 2019; dashed lines). The color version of this figure is available only in the electronic edition.

(HF) scatterograms (Mai *et al.*, 2010; Mena *et al.*, 2010; Olsen and Takedatsu, 2015). On the SCEC BBP, the LFs are input through the standard rupture format using a number of source realizations (e.g., 50) from Graves and Pitarka (2015) kinematic source generator module. The HF scatterograms are simulated for each of the three components of ground motion based on the theory for multiple scattering by Zeng *et al.* (1991, 1993), with user-specified site scattering parameters in a 1D velocity structure. The direct P -wave arrival time is found using 3D raytracing (Hole, 1992), after which the seismic-scattering wave energy appears. A source time function is then convolved with the scatterograms, assuming that the scattering operators and moment release originate throughout the fault but start at the hypocenter (Olsen and Takedatsu, 2015).

The SDSU module is available to generate input synthetics for structural seismic risk analysis, as one of the ground-motion generator modules of the SCEC BBP. However, the current SDSU module does not incorporate realistic interfrequency correlations into the simulations, as shown by the resulting interfrequency correlation coefficients for the Loma Prieta earthquake using the current SDSU module synthetics compared with the empirical result in Figure 2. At frequencies below the merging frequency between deterministic and stochastic signals (typically 1 Hz), the interfrequency correlations of epsilon show some promise, but the correlation is still much

lower than the empirical value. At frequencies above 1 Hz, the interfrequency correlations of epsilon are significantly lower than the empirical value and drop to almost zero moving away from the reference frequency. In the following, we develop and validate a method to implement interfrequency correlations of epsilon for FAS into the synthetics generated by the SDSU BBP module.

Inclusion of Interfrequency Correlation in the FAS

The empirical correlation available for this study is developed for the orientation-independent EAS, whereas our simulations generate separate components of ground motion. For that reason, we apply the EAS empirical correlation to the two horizontal components of FAS with assumptions about the relationship of the two components at the same station.

The procedure to generate a new ground-motion time series with realistic interfrequency correlations is as follows:

1. take the Fourier transform of the two horizontal components of the synthetic ground-motion time series. For each component, let the number of frequency points be n , the Fourier amplitude and phase at the i th frequency be $\text{Amp}_{\text{mean}}(i)$ and $\text{Ph}_{\text{mean}}(i)$, respectively;
2. for the two horizontal components 1 and 2, respectively, sample normally distributed vector-valued random variable R_{HC1} and R_{HC2} with zero mean, constant standard deviation σ , and size n . R_{HC1} and R_{HC2} can be independent or correlated with a correlation coefficient ρ_R . An illustration of R_{HC1} and R_{HC2} is shown in Figure 3a. Correlated R_{HC1} and R_{HC2} (R_{HC1}^c and R_{HC2}^c) can be generated by:

- express covariance matrix C of the two components:

$$C = \begin{bmatrix} 1 & \rho_R \\ \rho_R & 1 \end{bmatrix}, \quad (6)$$

- apply the Cholesky decomposition of covariance matrix C and obtain a 2×2 upper triangular matrix U as:

$$C = U^T U, \quad (7)$$

- right multiply matrix $[R_{\text{HC1}}, R_{\text{HC2}}]$ by U and obtain two correlated random variables R_{HC1}^c and R_{HC2}^c with correlation coefficient ρ_R :

$$[R_{\text{HC1}}^c, R_{\text{HC2}}^c] = [R_{\text{HC1}}, R_{\text{HC2}}]U, \quad (8)$$

in which $[R_{\text{HC1}}^c, R_{\text{HC2}}^c]$ and $[R_{\text{HC1}}, R_{\text{HC2}}]$ are n by 2 matrices with R_{HC1}^c or R_{HC1} as the first columns and R_{HC2}^c or R_{HC2} as the second columns, respectively. The upper triangular matrix is used here because the correlation is between the two columns of the matrix $[R_{\text{HC1}}^c, R_{\text{HC2}}^c]$. An illustration of R_{HC1}^c and R_{HC2}^c is shown in Figure 3b.

The following steps are the same for R_{HC1} and R_{HC2} (or R_{HC1}^c and R_{HC2}^c), so the HC1 and HC2 subscripts (or

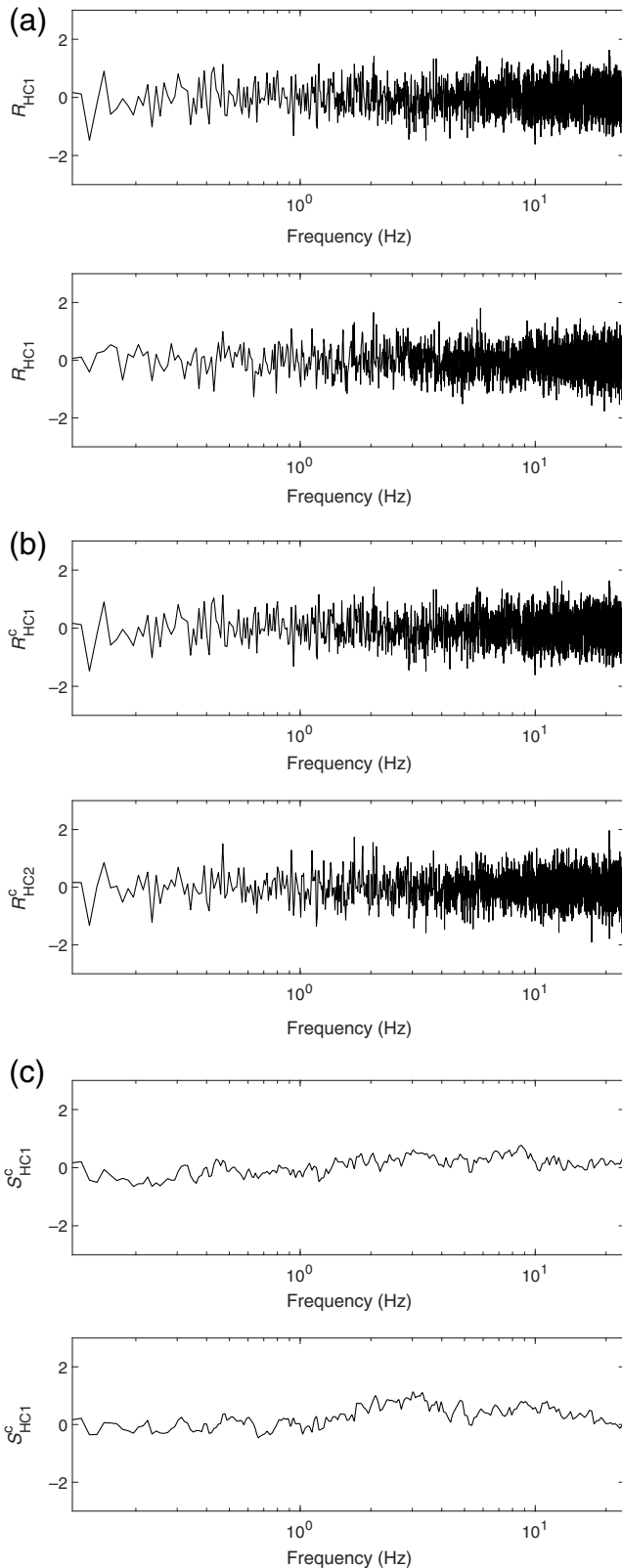


Figure 3. Illustration of steps (2–4) showing two independent normally distributed vector-valued random variables, corresponding to frequencies from 0.1 to 24 Hz for the two horizontal Fourier amplitude spectrum (FAS) components in terms of (a) R_{HC1} and R_{HC2} , (b) R_{HC1}^c and R_{HC2}^c , and (c) S_{HC1}^c and S_{HC2}^c .

superscript c) are dropped for notational brevity and R refers to either of the two random variables.

- express the empirical correlation $\rho_{\epsilon(f_1)\epsilon(f_2)}$ from equation (5) in matrix form Σ (n by n , real, symmetric, and positive definite), and apply the Cholesky decomposition of Σ as

$$\Sigma = LL^T, \quad (9)$$

in which L is a n by n lower triangular matrix (Seydel, 2012);

- left multiply random variable R in step (3) (within the corresponding frequency range 0.1–24 Hz) by L as

$$S = LR, \quad (10)$$

to generate a normal random variable S with zero mean and covariance equal to $\sigma^2 LL^T = \sigma^2 \Sigma$ (Seber and Lee, 2012). The lower triangular matrix is used here because the correlation is between the rows of R . An illustration of S_{HC1}^c and S_{HC2}^c is shown in Figure 3c. Here, for the corresponding frequency points outside the 0.1–24 Hz range, $S = R$;

- multiply the exponential of S with Amp_{mean} to compute the Fourier amplitude of the new ground-motion synthetics, Amp_{new} , as

$$\text{Amp}_{\text{new}}(i) = \text{Amp}_{\text{mean}}(i) \exp S_i; \quad (11)$$

- calculate the new ground-motion time series by applying the inverse Fourier transform to the amplitude spectrum obtained in step (5) and phase spectrum from step (1).

The method can be applied as the last step to simulate the ground motion using the SDSU SCEC BBP module. It maintains the mean of the natural logarithm of the Fourier amplitude for the updated ground-motion synthetics, since the mean of S_i in step (5) equals 0. Taking the natural logarithm of the equation in step (5) we get

$$\ln \text{Amp}_{\text{new}}(i) = \ln \text{Amp}_{\text{mean}}(i) + S_i. \quad (12)$$

We tested our method by calculating the within-event residual for simulations of the Loma Prieta earthquake using the SDSU broadband module (Olsen and Takedatsu, 2015) on the SCEC BBP. We generate 50 source realizations for the Loma Prieta earthquake using the kinematic source generator module by Graves and Pitarka (2015). These 50 source realizations have variations in hypocenter locations and slip distributions that are represented by the between-event residual. Here, we refer to each of the 50 source realizations as a separate event. For each event, we generate 10 simulations with imposed within-event interfrequency correlation at all the stations. The 10 simulations differ by the random variables (R_{HC1} and R_{HC2}) in step (2). The mean of the 10 simulations and their within-event residual is computed for each event, respectively. The within-event residual at all stations and all the 50 events are then

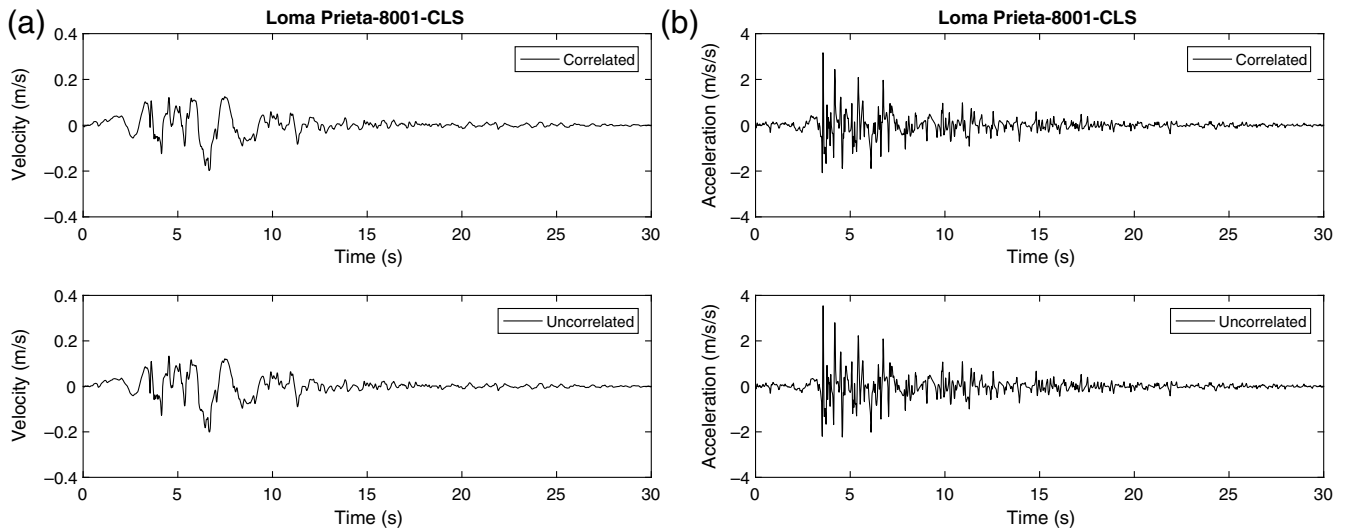


Figure 4. Examples of the north–south component of (a) velocities and (b) accelerations at station 8001-CLS for the Loma Prieta earthquake (top) after and (bottom) before implementing the interfrequency correlations.

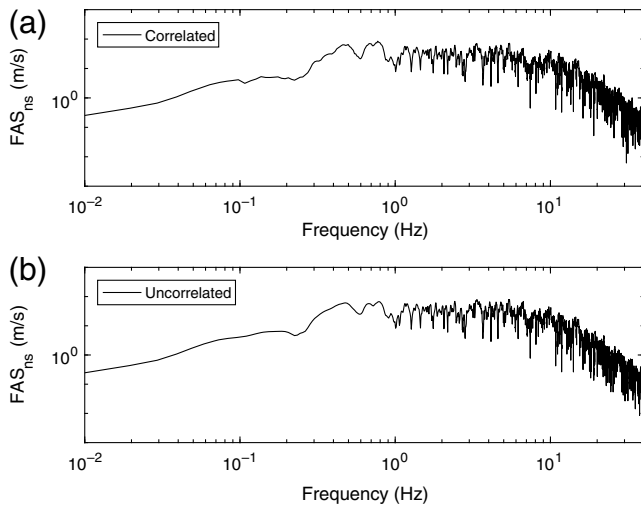


Figure 5. Examples of the north–south component of FAS for one simulation at station 8001-CLS for the Loma Prieta earthquake (a) after and (b) before implementing the interfrequency correlations.

pooled together at the corresponding frequencies. At each station and each frequency f , the epsilon of within-event residual $\epsilon(f)$ has a size of 500 (50 events \times 10 simulations). A total of 40 stations are used for the Loma Prieta earthquake in our simulations, so that the population of the epsilon of the within-event residual $\epsilon(f)$ at each frequency f is 20,000 (500 \times 40 stations).

This method generates correlated synthetic time series that are very similar to the original results from the current SDSU BBP module. Figures 4 and 5 show one component of synthetic time histories (velocity and acceleration) and FAS, respectively, at station 8001-CLS (see Fig. 6 for location) for the Loma Prieta earthquake before and after implementing

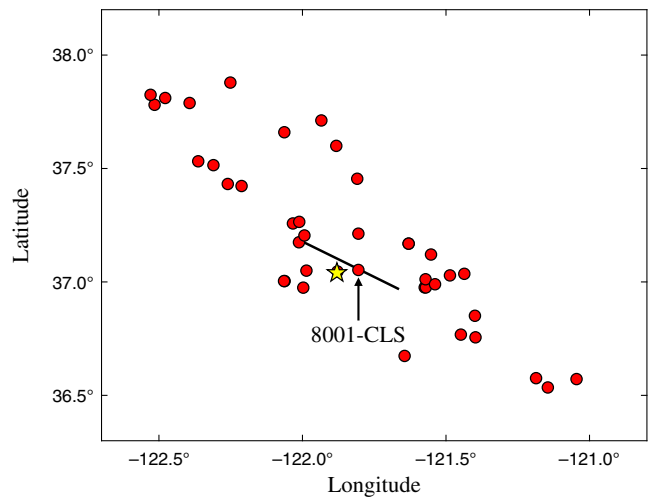


Figure 6. Location map for the Loma Prieta earthquake. The star depicts the epicenter, the bold line represents the fault trace, and the dots show the stations. Station 8001-CLS, where we compare time histories, is highlighted. Figure modified from Southern California Earthquake Center (SCEC) Broadband Platform (BBP) output. The color version of this figure is available only in the electronic edition.

the interfrequency correlations. A suite of 10 simulated EAS sequences for one of the 50 events at station 8001-CLS for the Loma Prieta earthquake with interfrequency correlation of the within-event residual implemented using this method is shown in Figure 7. Suites of 10 simulated EAS sequences for the rest of the 50 events at station 8001-CLS for the Loma Prieta earthquake are provided in [Figure S1](#), available in the supplemental material to this article. Figure 8a shows that the resulting interfrequency correlation coefficients obtained by our method (using independent R_{HC1} and R_{HC2} in step 2) for the Loma Prieta

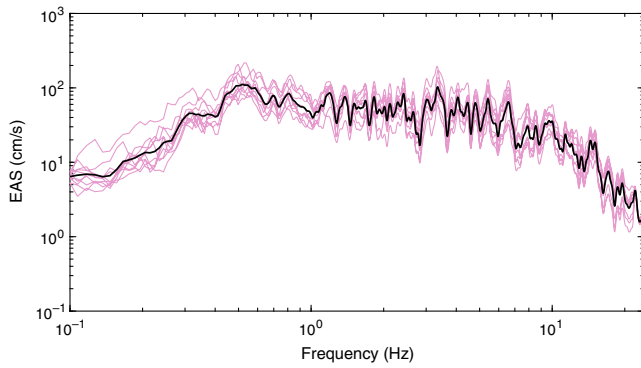


Figure 7. A suite of 10 simulated effective amplitude spectra (EAS) (thin light lines) with interfrequency correlation of the within-event residual implemented and their mean (bold black line) for one of the 50 events at station 8001-CLS for the Loma Prieta earthquake. Suites of 10 simulated EAS for the rest of the 50 events at station 8001-CLS for the Loma Prieta earthquake are provided in [Figure S1](#). The color version of this figure is available only in the electronic edition.

earthquake compare very well with the empirical result, as intended. [Figure 9](#) compares the bias (natural log misfit between the median observed and predicted PSA) for the uncorrelated and correlated SDSU synthetics. It is clear that the addition of correlation to the synthetic time histories results in insignificant changes in the bias. In other words, the method can be used as a postprocessing step to incorporate correlation into an already established and validated

ground-motion generator, without biasing the median spectral accelerations.

A small bias remains between the empirical values and the interfrequency correlation coefficients obtained by our method using independent R_{HC1} and R_{HC2} ([Fig. 8a](#)). This bias can be minimized using correlated R_{HC1} and R_{HC2} in step (2). [Baker and Jayaram \(2008\)](#) show that epsilon of response spectral accelerations for orthogonal components of ground motions is correlated, with correlation coefficients slightly dependent on period (0.7–0.9 for periods from 0.01 to 10 s). This result indicates that the different components of EAS ground motion (e.g., the two horizontal components) are also correlated. Because EAS is the square root of the mean power of the two horizontal components of FAS (FAS_{HC1} , FAS_{HC2}), implementation of correlated random variables R_{HC1} and R_{HC2} into FAS_{HC1} and FAS_{HC2} can indeed further improve the correlations in EAS. We generate R_{HC1} and R_{HC2} with correlation coefficient ρ_R equal to 0.7 at all frequencies in step (2) and compute the resulting interfrequency correlations in EAS (see [Fig. 8b](#)). The fit to the empirical value is further improved as compared with the interfrequency correlations in EAS using independent random variables for the two horizontal components. The value of the correlation coefficient here is chosen to provide an optimal fit in the final interfrequency correlation results and is similar to those described in [Baker and Jayaram \(2008\)](#). The resulting interfrequency correlation coefficients using other values of correlation coefficient between R_{HC1} and R_{HC2} are provided in [Figure S2–S4](#). These results

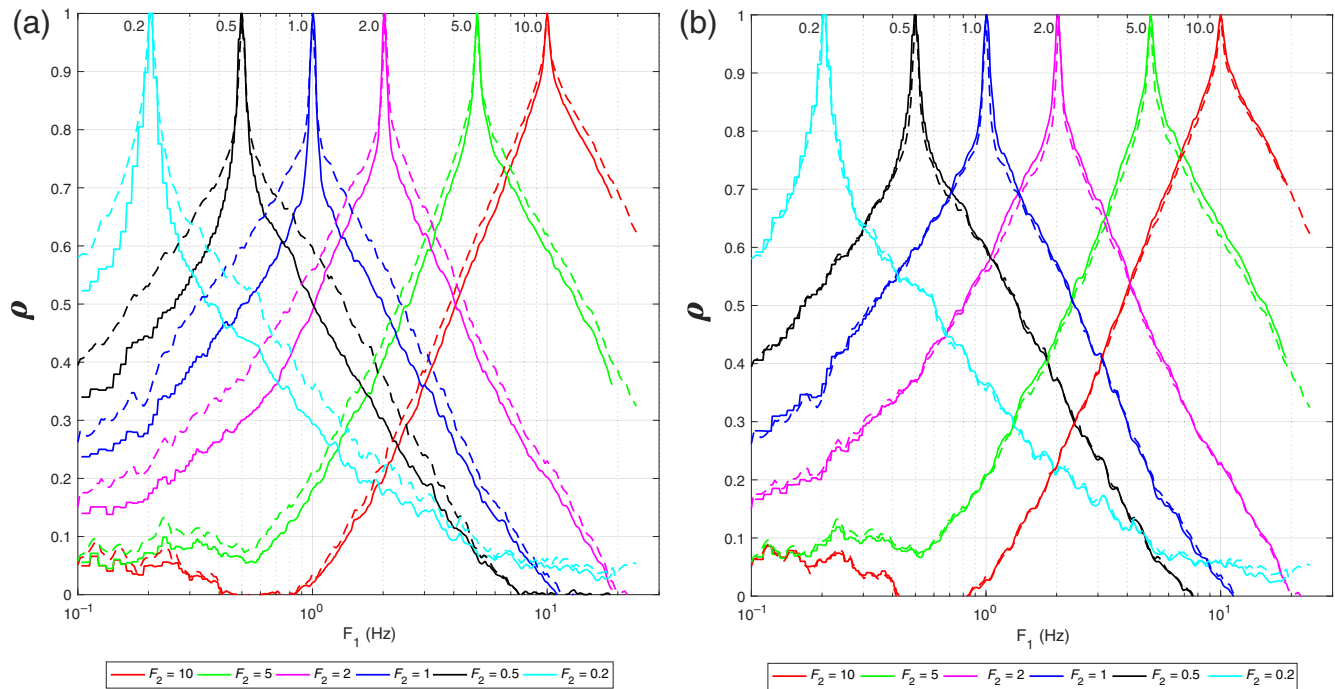


Figure 8. Interfrequency correlation coefficients of epsilon at reference frequencies 0.2, 0.5, 1, 2, 5, and 10 Hz from the empirical correlation coefficients ([Bayless and Abrahamson, 2019](#); dashed lines) and the SDSU SCEC BBP module (solid lines) after applying our method for two horizontal components using (a) independent random variables and (b) correlated random variables with a correlation coefficient of 0.7 for the Loma Prieta earthquake. The color version of this figure is available only in the electronic edition.

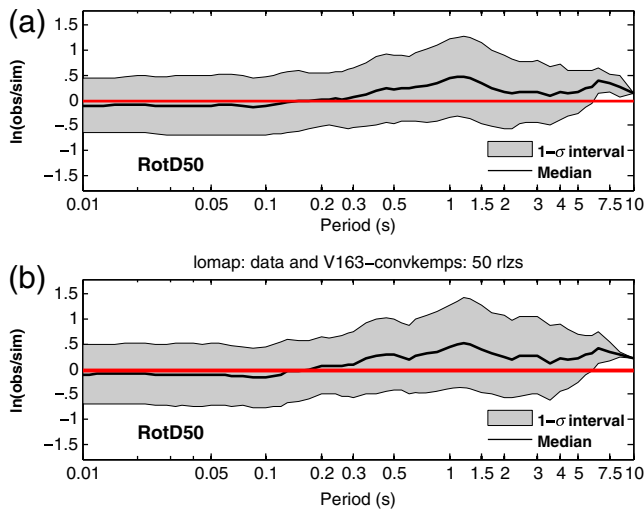


Figure 9. Logarithm misfit between the median observation of 50 source realizations and the median prediction for the (a) current and (b) improved SDSU synthetics for the Loma Prieta earthquake. The color version of this figure is available only in the electronic edition.

suggest that a correlation analysis between the FAS values of two orthogonal components may further improve the results.

Figures for the resulting interfrequency correlation coefficients from the other six western U.S. earthquakes are provided in (E) Figures S5–S10.

Discussion

We have developed and tested our method to include interfrequency correlation using the SCEC SDSU BBP code. However, the approach can easily be implemented in other simulation methods. The SDSU SCEC BBP module version 1.6.2 (v.1.6.2) has almost no correlation in the simulated result, so the empirical correlation matrix was applied directly on the broadband time histories with the desired results. If the method is applied to synthetic time histories that already include a level of interfrequency correlation different from that for empirical data, the correlation matrix Σ in step (3) can be adjusted accordingly. In addition, the empirical correlation coefficients used in this study are rather general without statistically significant magnitude, distance, site parameter, or regional dependencies (Bayless and Abrahamson, 2019). However, studies on the empirical correlations are on-going, and more parameter-specific results (e.g., for source and region) are likely to be obtained in the future. Including such updates into our method will be straightforward due to its flexible nature.

In our approach, the interfrequency correlations are only implemented into the amplitude spectrum in which we modify the Fourier amplitude while using the original phase spectrum (as is also the case for the correlation analysis of other methods, e.g., Stafford, 2017; Bayless and Abrahamson, 2018a). This is equivalent to applying a zero-phase filter to the uncorrelated synthetics to produce the correlated synthetics.

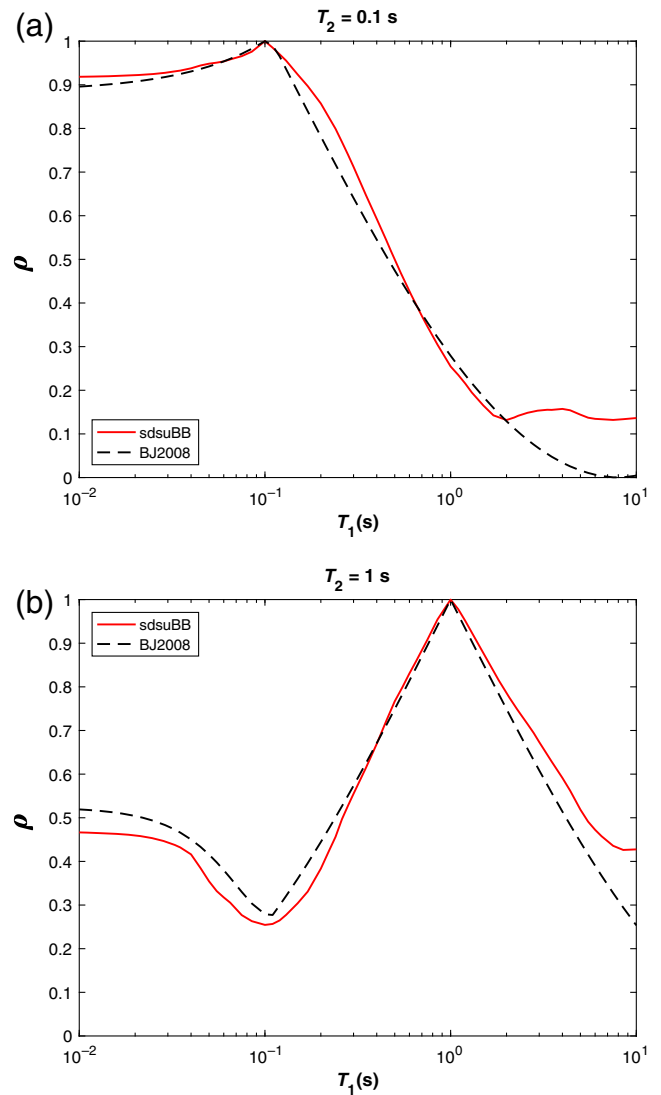


Figure 10. Comparison of the interfrequency spectral acceleration correlation coefficients of epsilon at reference periods (a) 0.1 s and (b) 1 s from the Baker and Jayaram (2008) model (dashed lines) and the SDSU SCEC BBP module after applying our method (solid lines) for the Loma Prieta earthquake with 50 simulations. The color version of this figure is available only in the electronic edition.

We also tested the use of a causal minimum-phase filter and obtained insignificant differences from the zero-phase filter in our application.

It is worth noting that the similarity on how S_i (step 5 of our method) and the within-event residual affect the interfrequency correlations. The value of the standard deviation σ in step (2) should be chosen such that it is consistent with the standard deviation of the original FAS. σ can also be implemented as frequency dependent if needed. For the SDSU SCEC BBP module, the same equations and scaling are used for simulating each component of the ground motions, thus σ is chosen to be the same for each component. However, other simulation methodologies may warrant different treatment of σ .

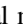
Figure 10 shows the resulting interfrequency correlation coefficients in response spectral accelerations obtained by our method for the Loma Prieta earthquake. The comparison shows a good level of agreement between our simulated result and the within-event correlation model regressed by Baker and Jayaram (2008). This result shows that implementing interfrequency correlations developed for FAS can also improve the correlation in spectral accelerations.

This method can be further enhanced to incorporate (frequency dependent) spatial correlations into the simulations by extending the correlated random variables in step (2) to 2D, to facilitate even more realistic seismic risk analysis. This effort, along with correlation analysis of the FAS components, is a part of an ongoing project.

Conclusions

We present a postprocessing method to introduce interfrequency correlations into seismic synthetic time histories, mimicking that seen in recorded ground motions, to allow more realistic seismic risk analysis. After implementing the correlation into the current SDSU SCEC BBP module, we show that the method generates correlated synthetic time series with interfrequency correlation that match that of empirical data very well. We show that incorporating the interfrequency correlation developed for the Fourier amplitudes also significantly improves the correlations in response spectral accelerations. Introducing the interfrequency correlation affects the median spectral accelerations insignificantly, and therefore retains the goodness of fit.

Data and Resources

Analyses and graphics production were performed using the numeric computing environment MATLAB (www.mathworks.com, last accessed May 2019). The empirical correlation coefficients table was provided by Jeff Bayless and Norman Abrahamson. Simulations in this article are performed using the Southern California Earthquake Center (SCEC) Broadband Platform (BBP) code. Figures showing examples of simulated effective amplitude spectrum (EAS), interfrequency correlation implemented in broadband synthetics for the Northridge, Landers, Chino Hills, North Palm Springs, Chino Hills, and Whittier events, and dependency of the results on the correlation between the two horizontal components are provided in the  supplemental material of this article.

Acknowledgments

This research was supported by the Southern California Earthquake Center (SCEC; Contribution Number 9932). SCEC is funded by National Science Foundation (NSF) Cooperative Agreement EAR-1600087 and U.S. Geological Survey (USGS) Cooperative Agreement G17AC00047. The authors are grateful to Jeff Bayless, two anonymous reviewers, Associate Editor Hiroshi Kawase, and Editor-in-Chief Thomas Pratt for useful review comments and suggestions that helped improve the article.

References

- Abrahamson, N. A., W. J. Silva, and R. Kamai (2014). Summary of the ASK14 ground motion relation for active crustal regions, *Earthq. Spectra* **30**, no. 3, 1025–1055.
- Akkar, S., M. A. Sandikkaya, and B. Ö. Ay (2014). Compatible ground-motion prediction equations for damping scaling factors and vertical-to-horizontal spectral amplitude ratios for the broader Europe region, *Bull. Earthq. Eng.* **12**, no. 1, 517–547.
- Al Atik, L., N. Abrahamson, J. J. Bommer, F. Scherbaum, F. Cotton, and N. Kuehn (2010). The variability of ground-motion prediction models and its components, *Seismol. Res. Lett.* **81**, no. 5, 794–801.
- Atkinson, G. M., and K. Assatourians (2015). Implementation and validation of EXSIM (a stochastic finite-fault ground-motion simulation algorithm) on the SCEC broadband platform, *Seismol. Res. Lett.* **86**, no. 1, 48–60.
- Azarbakhsh, A., M. Mousavi, M. Nourizadeh, and M. Shahri (2014). Dependence of correlations between spectral accelerations at multiple periods on magnitude and distance, *Eng. Struct. Dynam.* **43**, no. 8, 1193–1204.
- Baker, J. W., and B. A. Bradley (2017). Intensity measure correlations observed in the NGA-West2 database, and dependence of correlations on rupture and site parameters, *Earthq. Spectra* **33**, no. 1, 145–156.
- Baker, J. W., and C. A. Cornell (2006). Spectral shape, epsilon and record selection, *Earthq. Eng. Struct. Dynam.* **35**, no. 9, 1077–1095.
- Baker, J. W., and N. Jayaram (2008). Correlation of spectral acceleration values from NGA ground motion models, *Earthq. Spectra* **24**, no. 1, 299–317.
- Bayless, J., and N. A. Abrahamson (2018a). Evaluation of the interperiod correlation of ground-motion Simulations, *Bull. Seismol. Soc. Am.* **108**, no. 6, 3413–3430.
- Bayless, J., and N. A. Abrahamson (2018b). An empirical model for Fourier amplitude spectra using the NGA-West2 database, *PEER Report 2018/07*, Pacific Earthquake Engineering Research Center, University of California, Berkeley, California.
- Bayless, J., and N. A. Abrahamson (2019). An empirical model for the interfrequency correlation of epsilon for Fourier amplitude spectra, *Bull. Seismol. Soc. Am.* **109**, no. 3, 1058–1070.
- Boore, D. M. (2003). Simulation of ground motion using the stochastic method, *Pure Appl. Geophys.* **160**, nos. 3/4, 635–676.
- Boore, D. M., J. F. Gibbs, W. B. Joyner, J. C. Tinsley, and D. J. Ponti (2003). Estimated ground motion from the 1994 Northridge, California, earthquake at the site of the Interstate 10 and La Cienega Boulevard bridge collapse, West Los Angeles, California, *Bull. Seismol. Soc. Am.* **93**, no. 6, 2737–2751.
- Burks, L. S., and J. W. Baker (2014). Validation of ground-motion simulations through simple proxies for the response of engineered systems, *Bull. Seismol. Soc. Am.* **104**, no. 4, 1930–1946.
- Cimellaro, G. P. (2013). Correlation in spectral accelerations for earthquakes in Europe, *Earthq. Eng. Struct. Dynam.* **42**, no. 4, 623–633.
- Crempien, J. G., and R. J. Archuleta (2015). UCSB method for simulation of broadband ground motion from kinematic earthquake sources, *Seismol. Res. Lett.* **86**, no. 1, 61–67.
- Dreger, D. S., G. C. Beroza, S. M. Day, C. A. Goulet, T. H. Jordan, P. A. Spudich, and J. P. Stewart (2015). Validation of the SCEC broadband platform V14.3 simulation methods using pseudospectral acceleration data, *Seismol. Res. Lett.* **86**, no. 1, 39–47.
- Esposito, S., and I. Iervolino (2011). PGA and PGV spatial correlation models based on European multievent datasets, *Bull. Seismol. Soc. Am.* **101**, no. 5, 2532–2541.
- Fisher, R. A. (1958). *Statistical Methods for Research Workers*, Vol. 13, Hafner, Edinburgh, United Kingdom.
- Goda, K., and G. M. Atkinson (2009). Probabilistic characterization of spatially correlated response spectra for earthquakes in Japan, *Bull. Seismol. Soc. Am.* **99**, no. 5, 3003–3020.
- Goda, K., and H. P. Hong (2008). Spatial correlation of peak ground motions and response spectra, *Bull. Seismol. Soc. Am.* **98**, no. 1, 354–365.

- Goulet, C., N. Abrahamson, P. Somerville, and K. Wooddell (2015). The SCEC broadband platform validation exercise for pseudo-spectral acceleration: Methodology for code validation in the context of seismic hazard analyses, *Seismol. Res. Lett.* **86**, no. 1, 17–26.
- Goulet, C. A., A. Kottke, D. M. Boore, Y. Bozorgnia, J. Hollenback, T. Kishida, A. Der Kiureghian, O. J. Ktenidou, N. M. Kuehn, E. M. Rathje, *et al.* (2018). Effective amplitude spectrum (EAS) as a metric for ground motion modeling using Fourier amplitudes, *2018 Seismology of the Americas Meeting*, Miami, Florida, 14–17 May 2018.
- Graves, R., and A. Pitarka (2015). Refinements to the Graves and Pitarka (2010) broadband ground-motion simulation method, *Seismol. Res. Lett.* **86**, no. 1, 75–80.
- Heresi, P., and E. Miranda (2019). Uncertainty in intraevent spatial correlation of elastic pseudo-acceleration spectral ordinates, *Bull. Earthq. Eng.* **17**, no. 3, 1099–1115.
- Hole, J. A. (1992). Nonlinear high-resolution three-dimensional seismic travel time tomography, *J. Geophys. Res.* **97**, no. B5, 6553–6562.
- Jayaram, N., and J. W. Baker (2009). Correlation model for spatially distributed ground-motion intensities, *Earthq. Eng. Struct. Dynam.* **38**, no. 15, 1687–1708.
- Kawakami, H., and H. Mogi (2003). Analyzing spatial intraevent variability of peak ground accelerations as a function of separation distance, *Bull. Seismol. Soc. Am.* **93**, no. 3, 1079–1090.
- Konno, K., and T. Ohmachi (1998). Ground-motion characteristics estimated from spectral ratio between horizontal and vertical components of microtremor, *Bull. Seismol. Soc. Am.* **88**, no. 1, 228–241.
- Kottke, A., N. A. Abrahamson, D. M. Boore, Y. Bozorgnia, C. Goulet, J. Hollenback, T. Kishida, A. D. Kiureghian, O.-J. Ktenidou, N. Kuehn, *et al.* (2018). Selection of random vibration procedures for the NGA-East project, *PEER Report No. 2018/05*, Pacific Earthquake Engineering Research Center, University of California, Berkeley, California.
- Kutner, M. H., C. Nachtsheim, and J. Neter (2004). *Applied Linear Regression Models*, Fourth Ed., McGraw-Hill/Irwin, New York, New York.
- Loth, C., and J. W. Baker (2013). A spatial cross-correlation model of spectral accelerations at multiple periods, *Earthq. Eng. Struct. Dynam.* **42**, no. 3, 397–417.
- Mai, P. M., W. Imperatori, and K. B. Olsen (2010). Hybrid broadband ground-motion simulations: Combining long-period deterministic synthetics with high-frequency multiple S-to-S backscattering, *Bull. Seismol. Soc. Am.* **100**, no. 5A, 2124–2142.
- Markhvida, M., L. Ceferino, and J. W. Baker (2018). Modeling spatially correlated spectral accelerations at multiple periods using principal component analysis and geostatistics, *Earthq. Eng. Struct. Dynam.* **47**, no. 5, 1107–1123.
- Mena, B., P. M. Mai, K. B. Olsen, M. D. Purvance, and J. N. Brune (2010). Hybrid broadband ground-motion simulation using scattering Green's functions: Application to large-magnitude events, *Bull. Seismol. Soc. Am.* **100**, no. 5A, 2143–2162.
- Olsen, K. B., and R. Takedatsu (2015). The SDSU broadband ground-motion generation module BBtoolbox version 1.5, *Seismol. Res. Lett.* **86**, no. 1, 81–88.
- Seber, G. A., and A. J. Lee (2012). *Linear Regression Analysis*, John Wiley and Sons, Hoboken, New Jersey.
- Seydel, R. (2012). Generating random numbers with specified distributions, in *Tools for Computational Finance*, Universitext, Springer, London, United Kingdom.
- Sokolov, V., and F. Wenzel (2013). Further analysis of the influence of site conditions and earthquake magnitude on ground-motion within-earthquake correlation: Analysis of PGA and PGV data from the K-NET and the KiK-net (Japan) networks, *Bull. Earthq. Eng.* **11**, no. 6, 1909–1926.
- Sokolov, V., F. Wenzel, K.-L. Wen, and W.-Y. Jean (2012). On the influence of site conditions and earthquake magnitude on ground-motion within-earthquake correlation: Analysis of PGA data from TSMIP (Taiwan) network, *Bull. Earthq. Eng.* **10**, no. 5, 1401–1429.
- Stafford, P. J. (2017). Interfrequency correlations among Fourier spectral ordinates and implications for stochastic ground-motion simulation, *Bull. Seismol. Soc. Am.* **107**, no. 6, 2774–2791.
- Wang, M., and T. Takada (2005). Macrospectral correlation model of seismic ground motions, *Earthq. Spectra* **21**, no. 4, 1137–1156.
- Weatherill, G. A., V. Silva, H. Crowley, and P. Bazzurro (2015). Exploring the impact of spatial correlations and uncertainties for portfolio analysis in probabilistic seismic loss estimation, *Bull. Earthq. Eng.* **13**, no. 4, 957–981.
- Wesson, R. L., and D. M. Perkins (2001). Spatial correlation of probabilistic earthquake ground motion and loss, *Bull. Seismol. Soc. Am.* **91**, no. 6, 1498–1515.
- Wharf, C. A. (2016). Discrete multivariate representation of Fourier spectral ordinates, *M.Sc. Thesis.*, Imperial College London, Department of Civil and Environmental Engineering, London, United Kingdom.
- Zeng, Y., K. Aki, and T.-L. Teng (1993). Mapping of the high-frequency source radiation for the Loma Prieta earthquake, California, *J. Geophys. Res.* **98**, no. B7, 11,981–11,993.
- Zeng, Y., F. Su, and K. Aki (1991). Scattering wave energy propagation in a random isotropic scattering medium: 1. Theory, *J. Geophys. Res.* **96**, no. B1, 607–619.

Department of Geological Sciences
 San Diego State University
 5500 Campanile Drive
 San Diego, California 92182-1020 U.S.A.
 naw021@ucsd.edu

Manuscript received 30 May 2019;
 Published Online 29 October 2019